Heliyon 10 (2024) e24878

Contents lists available at ScienceDirect

Heliyon

journal homepage: www.cell.com/heliyon

Research article

Development and validation of a CT-based deep learning radiomics nomogram to predict muscle invasion in bladder cancer

Zongjie Wei [a,1], Huayun Liu [a,1], Yingjie Xv [a], Fangtong Liao [a], Quanhao He [a], Yongpeng Xie [a], Fajin Lv [b], Qing Jiang [c], Mingzhao Xiao [a,*]

[a] Department of Urology, The First Affiliated Hospital of Chongqing Medical University, Chongqing, China
[b] Department of Radiology, The First Affiliated Hospital of Chongqing Medical University, Chongqing, China
[c] Department of Urology, The Second Affiliated Hospital of Chongqing Medical University, Chongqing, China

ARTICLE INFO

Keywords:
Radiomics
Deep learning
Bladder cancer
Computed tomography
Nomogram

ABSTRACT

Objective: This study aimed to develop a nomogram combining CT-based handcrafted radiomics and deep learning (DL) features to preoperatively predict muscle invasion in bladder cancer (BCa) with multi-center validation.

Methods: In this retrospective study, 323 patients underwent radical cystectomy with pathologically confirmed BCa were enrolled and randomly divided into the training cohort (n = 226) and internal validation cohort (n = 97). And fifty-two patients from another independent medical center were enrolled as an independent external validation cohort. Handcrafted radiomics and DL features were constructed from preoperative nephrographic phase CT images. Least absolute shrinkage and selection operator (LASSO) regression was used to identify the most discriminative features in train cohort. Multivariate logistic regression was used to develop the predictive model and a deep learning radiomics nomogram (DLRN) was constructed. The predictive performance of models was evaluated by area under the curves (AUC) in the three cohorts. The calibration and clinical usefulness of DLRN were estimated by calibration curve and decision curve analysis.

Results: The nomogram that incorporated radiomics signature and DL signature demonstrated satisfactory predictive performance for differentiating non-muscle invasive bladder cancer (NMIBC) from muscle invasive bladder cancer (MIBC), with an AUC of 0.884 (95 % CI: 0.813–0.953) in internal validation cohort and 0.862 (95 % CI: 0.756–0.968) in external validation cohort, respectively. Decision curve analysis confirmed the clinical usefulness of the nomogram.

Conclusions: A CT-based deep learning radiomics nomogram exhibited a promising performance for preoperative prediction of muscle invasion in bladder cancer, and may be helpful in the clinical decision-making process.

1. Introduction

Bladder cancer is one of the most common malignant tumors of the urological tract, and the predominant histologic type is

* Corresponding author. Department of Urology, The First Affiliated Hospital of Chongqing Medical University, No. 1 Youyi Road, Yuzhong District, Chongqing, 400016, China.
E-mail address: mingzhaoxiao@cqmu.edu.cn (M. Xiao).
[1] These authors equally dedicated to this article.

https://doi.org/10.1016/j.heliyon.2024.e24878
Received 21 December 2023; Received in revised form 16 January 2024; Accepted 16 January 2024
Available online 17 January 2024

urothelial carcinoma [1]. Based on whether the tumor infiltrates the muscular layer or not, bladder cancer is classified into non-muscle invasive bladder cancer (NMIBC) and muscle invasive bladder cancer (MIBC) [2]. Approximately 70 % of new bladder cancer diagnoses are classified as NMIBC, which usually requires repeated endoscopic evaluation and resection [3]. MIBC accounts for approximately 25–30 % of new cases, for which radical cystectomy (RC) with pelvic lymph node dissection or with neoadjuvant therapy are the primary treatment [4]. Therefore, proper preoperative discrimination between NMIBC and MIBC is critical for treatment decisions and the improvement of patients' prognosis.

Currently, pathological examination of specimen obtained by transurethral resection of the bladder tumor (TURBT) or biopsy in the cystoscope is an important method to confirm the diagnosis and identify the depth of tumor infiltration [2]. However, the procedure is invasive and the result of tumor staging is influenced by the experience of the surgeon. Recently, the Vesical Imaging-Reporting and Data System (VI-RADS) based on multi-parametric magnetic resonance imaging (mpMRI) has be verified to have a favorable performance in identifying NMIBC between MIBC [[5,6]]. However, its accuracy is largely based on observer experience and proficiency in this scoring system, which is inevitably affected by interobserver variability. Although magnetic resonance imaging (MRI) has better soft tissue resolution than computed tomography (CT). MRI is more expensive, longer scanning time, not widely available in some primary hospitals, and not suitable for some patients with metal implants in the body or claustrophobia [7]. Therefore, it is still worthwhile to explore the potential utility of CT in predicting muscle invasion of bladder cancer.

Radiomics can provide non-invasive tools to identify tumor biological behavior by extracting and analyzing high-throughput quantitative data from medical images such as CT, MRI or positron emission tomography (PET) [8]. Recently, radiomics has made great progress in the automatic diagnosis of colorectal tumors, lung masses, breast diseases and some other diseases [9–14]. The usefulness of CT-based radiomics in differentiating histological variant [15], tumor grade [16] and stage [[17,18]] of bladder tumors has been demonstrated in previous studies, but these studies had some limitations, such as small sample size or no independent external validation set. In addition, deep learning (DL), widely used in image analysis, had the ability to extract deep and complex structures related to specific tasks, which had shown good performance in diagnosis and prognosis prediction for gastric, liver, and

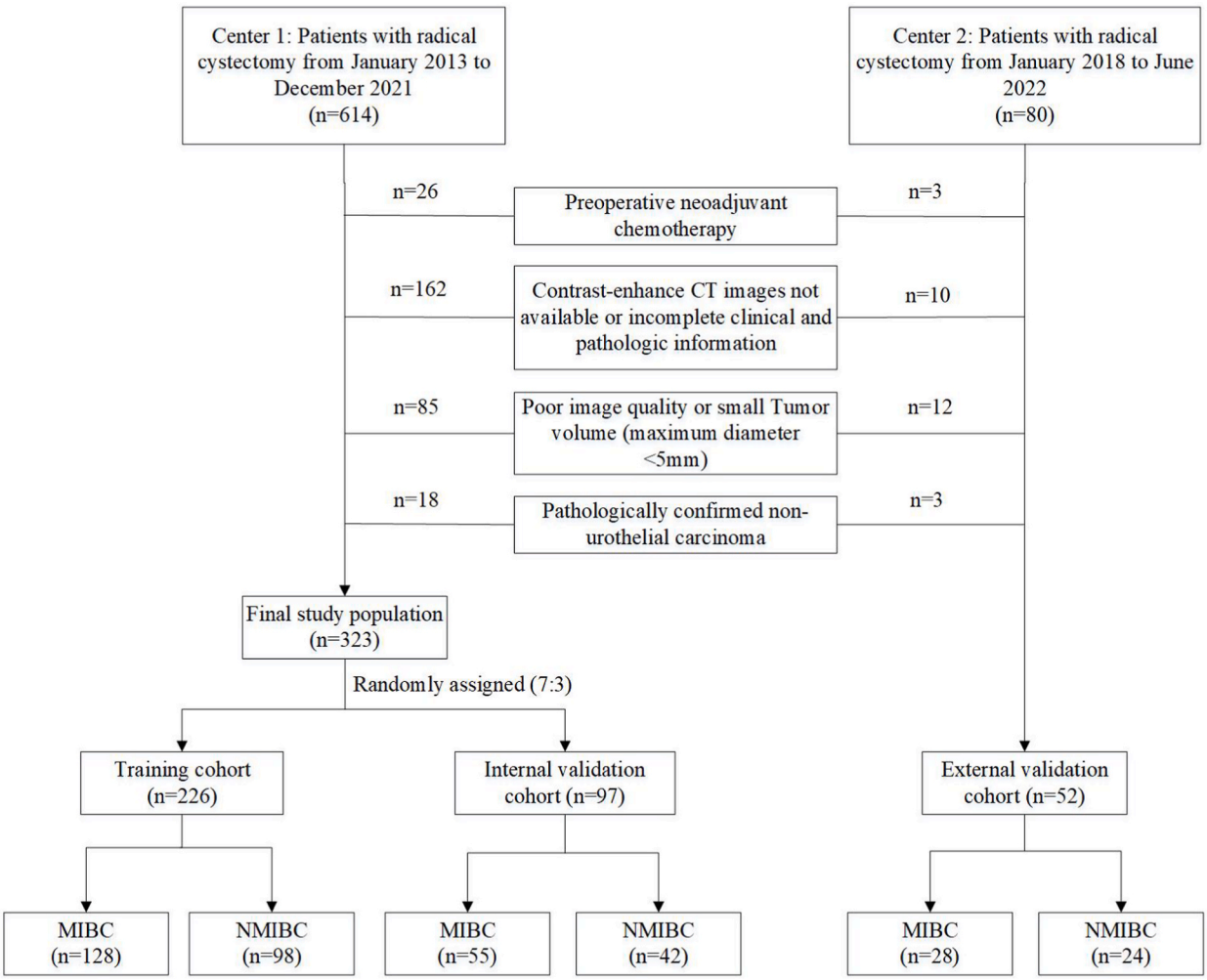

Fig. 1. The flowchart of the patient recruitment process.

renal cancers [19–21]. However, only a few studies have focused on the application of handcrafted radiomics combined with DL feature in predicting muscle invasion of bladder cancer. Therefore, we hypothesized that combining radiomics features and DL features would improve the diagnostic efficacy of the radiomics model.

Therefore, we aimed to develop and validate a deep learning radiomics nomogram (DLRN) combining CT-based handcrafted radiomics features and DL features to preoperatively predict muscle invasion in bladder cancer.

2. Patients and methods

2.1. Patients

This study was approved by our institutional review board, and the requirement for informed consent was waived. All the procedures were conducted in accordance with the Declaration of Helsinki. In primary center, we retrospectively included consecutive patients with bladder cancer who underwent radical cystectomy at center 1 between January 2013 and December 2021. The inclusion criteria were as follows: (1) underwent radical cystectomy and postoperative pathology confirmed urothelial carcinoma; (2) contrast-enhanced CT scan within 2 weeks prior to surgery. The exclusion criteria were as follows: (1) preoperative neoadjuvant chemotherapy; (2) contrast-enhance CT images not available or incomplete clinical and pathologic information; (3) poor CT imaging quality or small tumor volume (maximum diameter < 5 mm). Patients in the primary center were then randomly divided into a training cohort and an internal validation cohort in a 7:3 ratio using random numbers in R. The external independent validation cohort was enrolled in center 2 from January 2018 to June 2022, using the same criteria as the main cohort. The flowchart of the patient recruitment process is shown in Fig. 1. Clinical and pathological data were collected from the electronic medical record, including age, sex, relapse status, pathologic T stage, pathologic N stage and pathological grade. Pathologic tumor staging was performed according to the American Joint Committee on Cancer Staging Manual (8th edition) [22].

2.2. CT examination and image preprocess

CT scans were obtained within 2 weeks before the radical cystectomy. Nephrographic phase CT images were downloaded from Picture Archiving and Communication Systems (PACS) for subsequent analysis. The CT image acquisition settings details are shown in Supplementary Materials. Reader A (with more than 5 years of experience in the diagnosis of genitourinary diseases) using ITK-SNAP software manually segmented the three-dimensional (3D) region of interest (ROI) of the tumor, blinded to the pathological clinical information. If there were multiple lesions, the largest lesion was selected for image segmentation and feature extraction. To evaluate the radiomics feature extraction's inter- and intra-observer reproducibility, 30 images were randomly selected for ROI segmentation by Reader A after 2 weeks of the first segmentation and Reader B (with more than 10 years of experience in the diagnosis of genitourinary diseases) respectively. Two representative CT images of MIBC and NMIBC patients are exhibited in Supplementary Fig. 1.

2.3. Radiomics model construction

Using spline interference, all images were resampled to symmetrical voxels of 1*1*1 mm^3. CT-based feature extraction was performed using the pyradiomics package (version 2.2.0) in Python (version 3.7.1), according to the guidelines of the Image Biomarker Standardization Initiative (IBSI) [23]. Feature selection and radiomics signature construction were performed in train cohort according to the following steps: (i) all radiomics features were standardized separately using z-scores normalization; (ii) inter- and intra-class correlation coefficient (ICC) was used to evaluate the reproducibility of radiomics features, and the stable features (ICC >0.75) were selected for further analysis; (iii) features with significantly different in the NMIBC and MIBC groups were selected using independent samples *t*-test ($p < 0.05$); (iv) the least absolute shrinkage and selection operator (LASSO) regression algorithm with 5-fold cross-validation was used to selection the significant features; (v) radiomics signature was built by multivariate logistic regression analysis.

2.4. DL model construction

To make the DL model more focused on the spatial structure of the tumor itself, we first defined a 3D-cropbox for cropping out the region that contains only the tumor. The representative slice with the largest tumor ROI in cross-section was selected as input image and resized to 224*224 pixels. Training a deep learning model is computationally expensive and requires large number of images because of its millions of learnable parameters to estimate. To address the problem of insufficient data, we used the transfer learning technology to extract 1024 deep learning features based on the structure of ResNet-50 pre-trained on ImageNet [24]. All DL features were normalized by z-score normalization. The independent samples *t*-test and LASSO regression were used to select the most relevant features, and the DL signatures were constructed using multivariate logistic regression analysis.

2.5. Combined model construction

Finally, a combined model was constructed using multivariate logistic regression by combined the handcraft radiomics and DL signature. Additionally, a deep learning radiomics nomogram (DLRN) was constructed based on the final combined model.

2.6. Performance evaluation

The receiver operating characteristic (ROC) curve and the area under the ROC curve (AUC) value were used to evaluate the discrimination performance of established models in training, internal validation and external validation cohorts. The cutoff value identified by Youden index in the training cohort was used to calculated the accuracy (ACC), sensitivity (SEN), specificity (SPE), positive predictive value (PPV), and negative predictive value (NPV). Calibration curves were performed via bootstrapping with 1000 resamples to assess the discrimination of the combined model. Delong's test was used to compare the AUC of different models. Decision curve analysis (DCA) was used to evaluate the clinical utility of established models. The overall workflow of this study is summarized in Fig. 2.

2.7. Statistical analysis

Data analyses were performed using R (version 4.1.2; R Foundation for Statistical Computing; https://www.r-project.org) and the SPSS software (version 23.0; SPSS Inc., Chicago, IL, USA). R packages used in our study were shown in Supplementary Table 1. Continuous variables were presented as the means and standard deviation (SD), and categorical variables were presented as frequencies and percentages. Categorical and continuous variables were analyzed using the chi-square test and one-way ANOVA, respectively. All analyses were considered statistically significant with a two-sided *P*-value <0.05.

3. Results

3.1. Clinicopathological data

In center 1, a total of 323 patients were included in the final analysis, with 226 patients assigned to the training cohort (mean age, 65.86 $\pm$ 10.08 years [standard deviation]; 128 MIBC and 98 NMIBC) and 97 patients assigned to the internal validation cohort (mean age, 66.04 $\pm$ 9.56 years; 55 MIBC and 42 NMIBC). In center 2, 52 patients were enrolled as an independent external validation cohort (mean age, 65.44 $\pm$ 10.44 years; 28 MIBC and 24 NMIBC) to evaluate the generalization ability of the model. There were no significant differences in age, relapse status, CT-determined number of tumors, CT-determined tumor size, pathological T stage, pathological N stage and muscle invasion status between three cohorts. The clinical and pathological characteristics of the three cohorts are shown in Table 1.

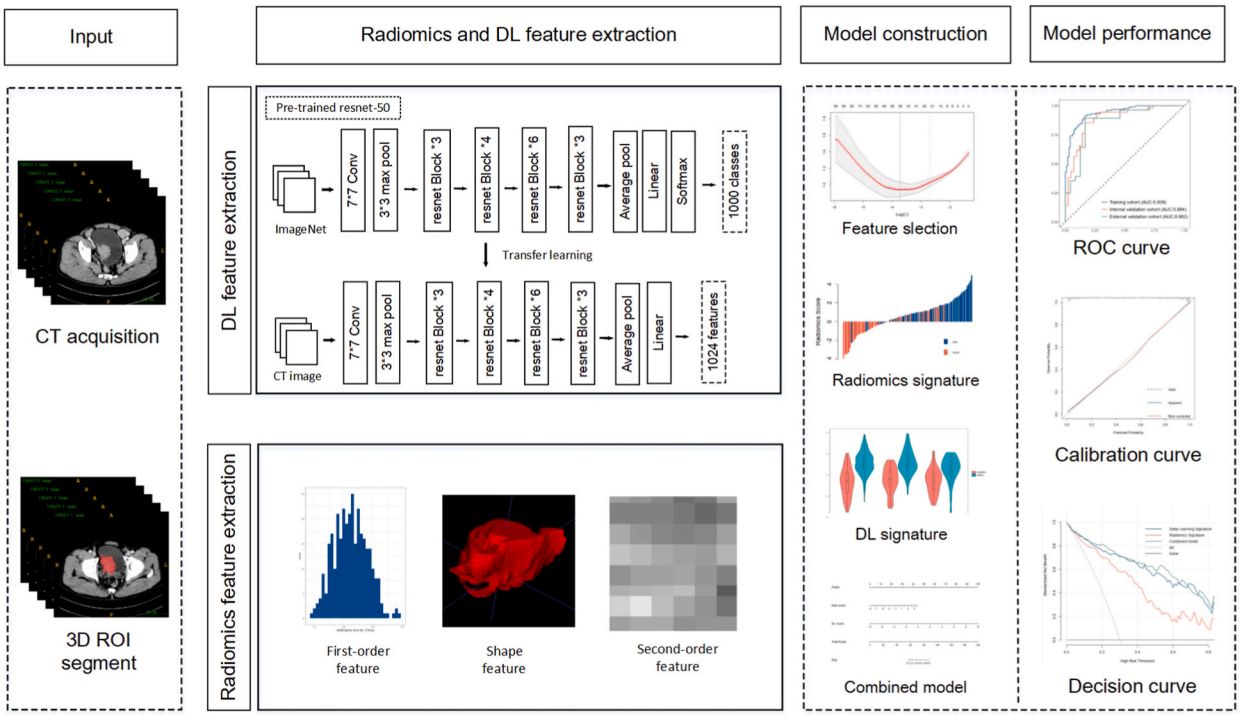

Fig. 2. The overall workflow of this study. CT: computed tomography, ROI: Region of interest, ROC: Receiver operating characteristic, DL: Deep learning.

3.2. Radiomics signature performance

A total of 1218 radiomics features were extracted from the nephrographic phase CT. 795 radiomics features showed a good inter- and intra-observer agreement with ICC >0.75. A total 319 radiomics features not associated with muscle invasion were excluded using the *t*-test. Finally, 11 significant radiomics features were identified and selected by LASSO regression model (Supplementary Fig. 2). The heat map of correlations between 11 radiomics features is shown in Supplementary Fig. 3. A significant difference was found in radiomics signature between MIBC and NMIBC patients in all cohorts (Fig. 3A). The radiomics signature yielded an AUC of 0.871 (95 % CI: 0.824–0.917) in training cohort, 0.840 (95 % CI: 0.763–0.918) in internal validation cohort and 0.807 (95 % CI: 0.683–0.930) in external validation cohort, respectively (Table 2).

3.3. DL signature performance

Finally, 1024 DL features were extracted from the nephrographic phase CT, and 22 features was selected to build the DL signature (Supplementary Fig. 4). As shown in Fig. 3B, there were significant differences in DL signature between the NMIBC and MIBC groups in all cohorts (all $P < 0.001$). The DL signature achieved better predictive performance than the handcrafted radiomics signature in training cohort (AUC, 0.929 vs 0.871, $p = 0.007$), internal validation cohort (AUC, 0.875 vs 0.840, $p = 0.386$) and external validation cohort (AUC, 0.843 vs 0.807, $p = 0.581$), respectively (Table 2).

3.4. Performance and validation of combined model

Multifactorial regression analysis showed that radiomics signature (OR: 1.529, 95%CI: 1.123–2.08) and DL signature (OR: 2.232, 95%CI: 1.69–2.948) were independent predictors of muscle invasion in bladder cancer. The nomogram incorporating radiomics signature and DL signature was shown in Fig. 5A. With the incorporation of radiomics signature, the combined model achieved a modest improvement over the single DL signature, with an AUC of 0.939 (95 % CI: 0.911–0.968) in training cohort, 0.884 (95 % CI: 0.813–0.953) in internal validation cohort and 0.862 (95 % CI: 0.756–0.968) in external validation cohort, respectively. According to DeLong's test, the difference between the combined model and the radiomic signature was statistically significant (AUC, 0.939 vs. 0.871, $p < 0.001$), but the difference between the combined model and the DL signature was not statistically significant (AUC, 0.939 vs. 0.929, $p = 0.061$) in the training cohort. Although no significant difference was observed between the models in the internal or external validation cohorts, the AUC of the combined model was higher than the two single-modality models. The ROC curves of three models in the internal validation and external validation cohorts were showed in Fig. 4A and B, respectively. The accuracy, sensitivity, specificity, negative predictive value and positive predictive value of different models for identifying patients with muscle invasion

Table 1
Comparison of clinical and pathological characteristics of the three cohorts.

Characteristic	Training cohort (n = 226)	Internal validation cohort(n = 97)	External validation cohort(n = 52)	p Value
Age	65.86 ± 10.08	66.04 ± 9.56	65.44 ± 10.44	0.941
Gender				<0.001
Male	209(92.5 %)	86(88.7 %)	37(71.2 %)	
Female	17(7.5 %)	11(11.3 %)	15(28.8 %)	
Relapse status				0.333
Yes	45(19.9 %)	19(19.6 %)	15(28.8 %)	
No	181(80.1 %)	78(80.4 %)	37(71.2 %)	
CT-determined number of tumors				0.346
Multiple	101(44.7 %)	35(36.1 %)	21(40.4 %)	
Single	125(55.3 %)	62(63.9 %)	31(59.6 %)	
CT-determined tumor size				0.620
<3 cm	55(24.3 %)	21(21.6 %)	15(28.8 %)	
≥3 cm	171(75.7 %)	76(78.4 %)	37(71.2 %)	
Pathological T-stage				0.934
Ta	25(11.1 %)	9(9.3 %)	7(13.5 %)	
T1	73(32.3 %)	33(34.0 %)	17(32.7 %)	
T2	74(32.7 %)	30(30.9 %)	18(34.6 %)	
T3	37(16.4 %)	18(18.6 %)	9(17.3 %)	
T4	17(7.5 %)	7(7.2 %)	1(1.9 %)	
Pathological N-stage[a]				0.405
N0	87(84.5 %)	46(88.5 %)	46(92.0 %)	
N1	16(15.5 %)	6(11.5 %)	4(8.0 %)	
Pathological grade				0.019
Low	36(15.9 %)	13(13.4 %)	16(30.8 %)	
High	190(84.1 %)	84(86.8 %)	36(69.2 %)	
Muscle invasion				0.931
MIBC	128(56.6 %)	55(56.7 %)	28(53.8 %)	
NMIBC	98(43.4 %)	42(43.3 %)	24(46.2 %)	

[a] Only patients with pelvic lymph node dissection were counted.

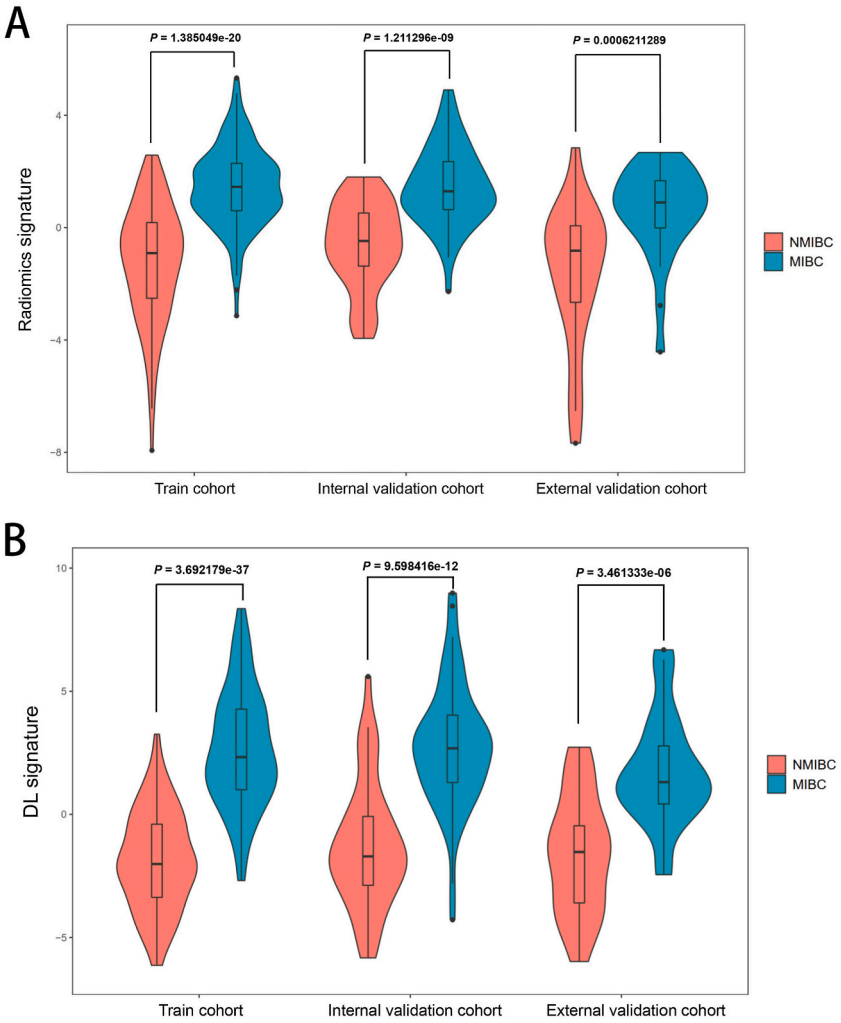

Fig. 3. Violin plots of radiomics signature and DL signature in the training, internal validation and external validation cohorts. (A) A significant difference was found in radiomics signature between MIBC and NMIBC patients in the training (mean, 1.455 vs. −1.389, $p < 0.001$), internal validation (mean, 1.464 vs. −0,617, $p < 0.001$) and external validation cohorts (mean, 0.621 vs. −1.627, $p < 0.001$). (B) A significant difference was found in DL signature between MIBC and NMIBC patients in the training (mean, 2.639 vs. −1.879, $p < 0.001$), internal validation (mean, 2.909 vs. −1.289, $p < 0.001$) and external validation cohorts (mean, 1.733 vs. −1.644, $p < 0.001$).

Table 2
Comparison of the performance of three models in training, internal validation and external validation cohorts.

Models		AUC	ACC	SEN	SPE	PPV	NPV
Training cohort	Radiomics signature	0.871(0.824–0.917)	0.82	0.90	0.71	0.80	0.84
	Deep Learning signature	0.929(0.897–0.961)	0.86	0.83	0.9	0.91	0.8
	Combined model	0.939(0.911–0.968)	0.88	0.91	0.84	0.88	0.88
Internal validation cohort	Radiomics signature	0.840(0.763–0.918)	0.75	0.87	0.6	0.74	0.78
	Deep Learning signature	0.875(0.780–0.950)	0.85	0.85	0.83	0.87	0.81
	Combined model	0.884(0.813–0.953)	0.85	0.95	0.71	0.81	0.91
External validation cohort	Radiomics signature	0.807(0.683–0.930)	0.73	0.75	0.71	0.75	0.71
	Deep Learning signature	0.843(0.731–0.957)	0.73	0.68	0.79	0.79	0.68
	Combined model	0.862(0.756–0.968)	0.85	0.89	0.79	0.83	0.86

AUC: area under the receiver operating characteristic curve; ACC: accuracy; SEN: sensitivity; SPE: specificity; PPV: positive predictive value; NPV: negative predictive value.

were summarized in Table 2. The calibration curve showed good calibration in the internal and external validation cohorts (Fig. 5B and C). The DCA demonstrated that, throughout the majority range of threshold probabilities, the patients would benefit more from using the combined model than the treat-none strategy or the treat-all-patients strategy and radiomics-only signature (Fig. 5D).

4. Discussion

In the present study, we developed and validated a CT-based deep learning radiomics nomogram to predict muscle invasion of bladder cancer based on retrospective data from 375 patients at two independent centers, which provides a novel non-invasive tool for the preoperative staging of bladder cancer. Our study demonstrated that the enhanced CT-based radiomics features and DL features were able to reflect the muscle infiltration characteristics of bladder cancer. Meanwhile, DLRN offers clinicians a simple-to-use, measurable, and individualized tool to forecast the likelihood of muscle invasion in bladder cancer.

MIBC is characterized by high mortality and poor prognosis, and radical cystectomy is its primary treatment [2]. Therefore, proper staging is crucial for therapeutic decisions and prognosis for bladder cancer patients. However, the current usual clinical staging approaches, including CT, MRI, and TURBT, are insufficient, and it is estimated that approximately half of patients undergoing radical cystectomy are clinically understaged [7]. TURBT is a commonly used preoperative staging method, but its diagnostic efficacy is related to the experience of the surgeon, and it is an invasive procedure with risks of infection, bleeding, and pain.

Radiomics provides a non-invasive automated method to diagnose, stage, and predict the prognosis of tumors by quantitatively extracting large amounts of features from radiographic images that are not observable to our naked eye [25]. Several studies have reported the promising predictive performance of MRI-based radiomics in preoperatively discriminating between NMIBC and MIBC [26–29]. Previous studies have shown that radiomics features extracted from CT can also predict muscular infiltration status in bladder cancer, but most of them were either very small sample sizes [[17,18,30]] or lacked independent external validation [31]. Our study also demonstrated that radiomics signature alone had promising discriminatory performance in preoperative clinical staging of bladder cancer, with AUCs of 0.840 (95 % CI 0.763–0.918) in the internal validation cohort and 0.807 (95 % CI 0.683–0.930) in the internal validation cohort. However, few studies have focused on deep learning techniques to preoperatively discriminate MIBC from NMIBC.

In the present study, a deep learning method based on the ResNet-50 architecture was used for DL feature extraction. The DL signature in our study presented a more promising performance than handcraft radiomics features. The AUC of the DL signature was significantly higher than the radiomics signature in the training set (0.929 vs 0.871, $p = 0.007$). Although, there was no significant difference in the internal and external validation cohorts, the AUC values of the DL signature were slightly increased to 0.875 and 0.843, respectively. The predictive performances of established DL signature were similar to the study published by zhang et al. [32]. However, the results differed from the findings of Chen et al. [33] which showed that DL features were less effective than radiomics-only model (AUC of 0.769 vs 0.782 in the test set). One possible reason is that prior to transfer learning and feature extraction, we designed the 3D-cropbox structure to remove the background outside the tumor region to focus the DL model on the spatial structure of the tumor itself. DL can improve the performance by mining high-dimensional imaging features in enhanced CT, which provide enriched information reflecting tumor spatial heterogeneity and tumor microenvironment. Moreover, with the incorporation of radiomics signature, the combined model achieved a modest improvement over the single DL signature, with an AUC of 0.884 in the internal validation cohort and 0.862 in the independent external validation cohort. Although the AUC improvement of the combined model is marginal, the accuracy and sensitivity of the model in the external test set are greatly improved. This suggests that handcrafted radiomics features can provide additional muscle infiltration information, which complements deep learning

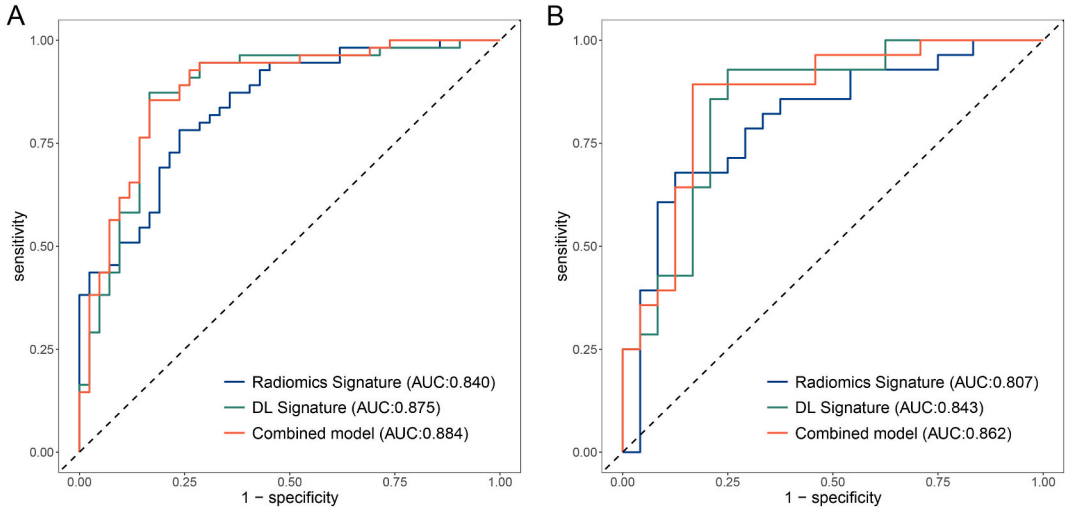

Fig. 4. The receiver operating characteristic (ROC) curves of three models in the internal validation (A) and external validation cohorts (B).

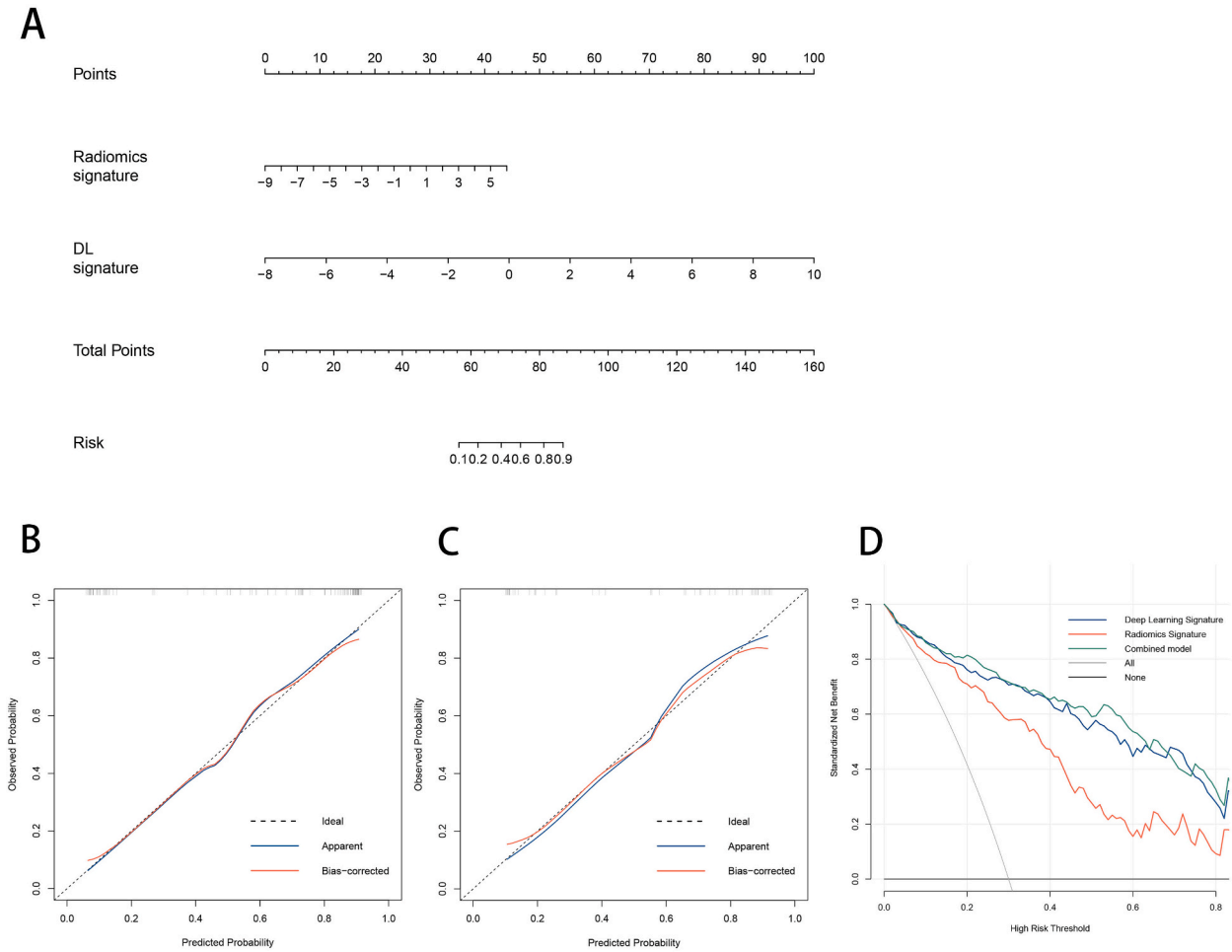

Fig. 5. The deep learning radiomics nomogram, calibration curves and decision curve analysis. (A) The nomogram, incorporating radiomics signature and DL signature, developed in the training cohort. The calibration curve showed good calibration in internal validation cohort (B) and external validation cohort (C). The DCA demonstrated that, throughout the majority range of threshold probabilities, the patients would benefit more from using the combined model than the treat-none strategy or the treat-all-patients strategy and radiomics-only signature (D).

features. Therefore, we constructed a nomogram based on the combined predictive model, which can provide clinicians with an easy, quantifiable tool to make clinical decisions. The combined model also showed good calibration in the training and internal validation and external validation cohorts.

It is also noteworthy that most procedures for obtaining pathological specimens in previous studies used TURBT alone [29], or TURBT in combination with radical cystectomy [28,31,33,34]. However, TURBT may provide uncertain or incorrect pathological staging of tumors due to the risk of surgical specimens not containing muscle layers or degeneration of tissue damage caused by electrothermal radiation [35]. In this study, the outcome indicators of the model were all based on pathological examination after radical cystectomy, which is the gold standard for accurate staging of bladder cancer.

The present study also has some limitations. First, the training data for our model were retrospectively collected from our hospital with a small sample size, and it was inevitably subject to selection bias. Second, our model incorporated both deep learning features and handcrafted radiomics features, with the potential for overfitting. Although the discrimination performance of the model was validated using data from an independent external medical center, all patients enrolled in the present study were from an administrative district in southwest China. Therefore, the generalization ability of the present model requires further evaluation in the cross-regional, multi-center and prospective data. Third, the present study did not include genetic markers, which could potentially improve the discrimination performance for muscle invasion. Finally, the ROI was manually segmented by radiologists, and the segmentation results may be subjectively biased, which may affect the stability and reproducibility of the study results.

5. Conclusion

In conclusion, handcrafted radiomics and DL features based on contrast-enhanced CT were able to preoperatively predict muscle

invasion of bladder cancer. The DL signature presented a more promising performance than handcraft radiomics features. A CT-based deep learning radiomics nomogram exhibited satisfactory discrimination performance and may be helpful in the clinical decision-making process.

Ethics approval and consent to participate

This study was approved by the Ethics Committee of The First Affiliated Hospital of Chongqing Medical University (Approval No. 2022-K508), and the requirement for informed consent was waived due to the retrospective nature of the study.

Data availability statement

The datasets analyzed during the current study are not publicly available due to the need for follow-up research but are available from the corresponding author on reasonable request.

Funding

This work was supported by the Chongqing Talent Program [grant number CQYC202003].

CRediT authorship contribution statement

Zongjie Wei: Writing – original draft, Software, Methodology, Data curation. **Huayun Liu:** Writing – original draft, Data curation. **Yingjie Xv:** Writing – review & editing. **Fangtong Liao:** Data curation. **Quanhao He:** Software, Methodology. **Yongpeng Xie:** Data curation. **Fajin Lv:** Conceptualization. **Qing Jiang:** Data curation, Conceptualization. **Mingzhao Xiao:** Writing – review & editing, Supervision, Funding acquisition, Conceptualization.

Declaration of competing interest

The authors declare that they have no known competing financial interests or personal relationships that could have appeared to influence the work reported in this paper.

Appendix A. Supplementary data

Supplementary data to this article can be found online at https://doi.org/10.1016/j.heliyon.2024.e24878.

References

[1] R.L. Siegel, K.D. Miller, H.E. Fuchs, A. Jemal, Cancer statistics, 2022, CA Cancer J Clin 72 (2022) 7–33.
[2] A.T. Lenis, P.M. Lec, K. Chamie, M.D. Mshs, Bladder cancer: a review, JAMA 324 (2020) 1980–1991.
[3] B. Jordan, J.J. Meeks, T1 bladder cancer: current considerations for diagnosis and management, Nat. Rev. Urol. 16 (2019) 23–34.
[4] V.G. Patel, W.K. Oh, M.D. Galsky, Treatment of muscle-invasive and advanced bladder cancer in 2020, CA Cancer J Clin 70 (2020) 404–423.
[5] C. Luo, B. Huang, Y. Wu, J. Chen, L. Chen, Use of Vesical Imaging-Reporting and Data System (VI-RADS) for detecting the muscle invasion of bladder cancer: a diagnostic meta-analysis, Eur. Radiol. 30 (2020) 4606–4614.
[6] V. Panebianco, Y. Narumi, E. Altun, et al., Multiparametric magnetic resonance imaging for bladder cancer: Development of VI-RADS (Vesical imaging-reporting and data system), Eur. Urol. 74 (2018) 294–306.
[7] P.J. Hensley, V. Panebianco, E. Pietzak, et al., Contemporary staging for muscle-invasive bladder cancer: accuracy and limitations, Eur Urol Oncol (2022), https://doi.org/10.1016/j.euo.2022.04.008.
[8] M.E. Mayerhoefer, A. Materka, G. Langs, et al., Introduction to radiomics, J. Nucl. Med. 61 (2020) 488–495.
[9] J. Shin, N. Seo, S.E. Baek, et al., MRI radiomics model predicts pathologic complete response of rectal cancer following chemoradiotherapy, Radiology (2022), https://doi.org/10.1148/radiol.211986:211986.
[10] Y. Yu, Z. He, J. Ouyang, et al., Magnetic resonance imaging radiomics predicts preoperative axillary lymph node metastasis to support surgical decisions and is associated with tumor microenvironment in invasive breast cancer: a machine learning, multicenter study, EBioMedicine 69 (2021) 103460.
[11] L. Yang, D. Gu, J. Wei, et al., A radiomics nomogram for preoperative prediction of microvascular invasion in hepatocellular carcinoma, Liver Cancer 8 (2019) 373–386.
[12] H. Zhang, X. Li, Y. Zhang, et al., Diagnostic nomogram based on intralesional and perilesional radiomics features and clinical factors of clinically significant prostate cancer, J. Magn. Reson. Imag. 53 (2021) 1550–1558.
[13] Y.Q. Huang, C.H. Liang, L. He, et al., Development and validation of a radiomics nomogram for preoperative prediction of lymph node metastasis in colorectal cancer, J. Clin. Oncol. 34 (2016) 2157–2164.
[14] Y.M. Zheng, W.J. Xu, D.P. Hao, et al., A CT-based radiomics nomogram for differentiation of lympho-associated benign and malignant lesions of the parotid gland, Eur. Radiol. 31 (2021) 2886–2895.
[15] S. Evrimler, M. Ali Gedik, T. Ahmet Serel, O. Ertunc, S. Alperen Ozturk, S. Soyupek, Bladder urothelial carcinoma: machine learning-based computed tomography radiomics for prediction of histological variant, Acad. Radiol. (2022), https://doi.org/10.1016/j.acra.2022.02.007.
[16] G. Zhang, L. Xu, L. Zhao, et al., CT-based radiomics to predict the pathological grade of bladder cancer, Eur. Radiol. 30 (2020) 6749–6756.
[17] Q. Zhou, Z. Zhang, X. Ang, H. Zhang, J. Ouyang, A nomogram combined with radiomics features, albuminuria, and metabolic syndrome to predict the risk of myometrial invasion of bladder cancer, Transl. Cancer Res. 10 (2021) 3177–3191.
[18] S.S. Garapati, L. Hadjiiski, K.H. Cha, et al., Urinary bladder cancer staging in CT urography using machine learning, Med. Phys. 44 (2017) 5814–5823.

[19] Y. Cui, J. Zhang, Z. Li, et al., A CT-based deep learning radiomics nomogram for predicting the response to neoadjuvant chemotherapy in patients with locally advanced gastric cancer: a multicenter cohort study, EClinicalMedicine 46 (2022) 101348.
[20] C. An, D. Li, S. Li, et al., Deep learning radiomics of dual-energy computed tomography for predicting lymph node metastases of pancreatic ductal adenocarcinoma, Eur J Nucl Med Mol Imaging 49 (2022) 1187–1199.
[21] K.H. Uhm, S.W. Jung, M.H. Choi, et al., Deep learning for end-to-end kidney cancer diagnosis on multi-phase abdominal computed tomography, npj Precis. Oncol. 5 (2021) 54.
[22] M.B. Amin, F.L. Greene, S.B. Edge, et al., The Eighth Edition AJCC Cancer Staging Manual: continuing to build a bridge from a population-based to a more "personalized" approach to cancer staging, CA Cancer J Clin 67 (2017) 93–99.
[23] A. Zwanenburg, M. Vallières, M.A. Abdalah, et al., The image biomarker standardization initiative: standardized quantitative radiomics for high-throughput image-based phenotyping, Radiology 295 (2020) 328–338.
[24] K. He, X. Zhang, S. Ren, J. Sun, Deep residual learning for image recognition, in: Proceedings of the IEEE Conference on Computer Vision and Pattern Recognition, 2016, pp. 770–778.
[25] P. Lambin, E. Rios-Velazquez, R. Leijenaar, et al., Radiomics: extracting more information from medical images using advanced feature analysis, Eur. J. Cancer 48 (2012) 441–446.
[26] Y. Liu, X. Xu, H. Wang, et al., The additional value of tri-parametric MRI in identifying muscle-invasive status in bladder cancer, Acad. Radiol. 30 (2023) 64–76.
[27] S. Xu, Q. Yao, G. Liu, et al., Combining DWI radiomics features with transurethral resection promotes the differentiation between muscle-invasive bladder cancer and non-muscle-invasive bladder cancer, Eur. Radiol. 30 (2020) 1804–1812.
[28] J. Zheng, J. Kong, S. Wu, et al., Development of a noninvasive tool to preoperatively evaluate the muscular invasiveness of bladder cancer using a radiomics approach, Cancer 125 (2019) 4388–4398.
[29] X. Xu, X. Zhang, Q. Tian, et al., Quantitative identification of nonmuscle-invasive and muscle-invasive bladder carcinomas: a multiparametric MRI radiomics analysis, J. Magn. Reson. Imag. 49 (2019) 1489–1498.
[30] Z. Wang, Y. He, N. Wang, et al., Clinical value of texture analysis in differentiation of urothelial carcinoma based on multiphase computed tomography images, Medicine (Baltim.) 99 (2020) e20093.
[31] Y. Cui, Z. Sun, X. Liu, X. Zhang, X. Wang, CT-based radiomics for the preoperative prediction of the muscle-invasive status of bladder cancer and comparison to radiologists' assessment, Clin. Radiol. (2022), https://doi.org/10.1016/j.crad.2022.02.019.
[32] G. Zhang, Z. Wu, L. Xu, et al., Deep learning on enhanced CT images can predict the muscular invasiveness of bladder cancer, Front. Oncol. 11 (2021) 654685.
[33] W. Chen, M. Gong, D. Zhou, et al., CT-based deep learning radiomics signature for the preoperative prediction of the muscle-invasive status of bladder cancer, Front. Oncol. 12 (2022) 1019749.
[34] G. Zhang, Z. Wu, X. Zhang, et al., CT-based radiomics to predict muscle invasion in bladder cancer, Eur. Radiol. (2022), https://doi.org/10.1007/s00330-021-08426-3.
[35] M.G.K. Cumberbatch, B. Foerster, J.W.F. Catto, et al., Repeat transurethral resection in non-muscle-invasive bladder cancer: a systematic review, Eur. Urol. 73 (2018) 925–933.